AAS 22-603

A MOTION PRIMITIVE APPROACH TO TRAJECTORY DESIGN IN A MULTI-BODY SYSTEM

Thomas R. Smith* **and Natasha Bosanac†**

This paper presents a motion primitive approach to trajectory design in multi-body systems. Motion primitives sampled from fundamental solutions, e.g. periodic orbits and stable/unstable manifolds, supply a discrete summary of segments of the phase space. Graphs of motion primitives are constructed and searched to produce primitive sequences that form candidate initial guesses for transfers of distinct geometries. Transfers are then computed from each initial guess using multi-objective constrained optimization. This approach is used to construct transfers in the Earth-Moon circular restricted three-body problem with impulsive maneuvers, demonstrating the potential for a primitive-based approach to support rapid and efficient trajectory design.

1 INTRODUCTION

A challenging aspect of trajectory design in multi-body systems is developing a systematic, rapid, and robust process for initial guess construction. The difficulty of constructing an initial guess depends on the complexity of the design space and the quality of the initial guess impacts the ability to recover a feasible solution. Even in a low-fidelity approximation of a multi-body gravitational environment, such as the circular restricted three-body problem (CR3BP), the available design space is large and analytical solutions do not exist.[1] Consequently, initial guess construction may become a challenging and potentially time-consuming task for the trajectory designer, particularly when there are significant constraints derived from mission requirements or hardware parameters. To guide initial guess construction for complex trajectories in a chaotic multi-body gravitational system, Smith and Bosanac have recently introduced a motion primitive approach to trajectory design.[2,3]

In the field of robotics, motion primitives have been used to construct complex paths. Wolek and Woolsey describe a motion primitive as a "feasible trajectory that is used as a fundamental building block to construct more complex paths".[4] This concept is often used in robotics to reduce the complexity of motion planning.[4,5] As an example, Frazzoli et al. form a finite library of trim and maneuver primitives for motion planning in time invariant dynamical systems.[6] In their work, a motion plan is defined as a sequence of concatenated motion primitives where a finite-state machine, denoted as a maneuver automaton, is represented as a graph and governs how primitives can be assembled into a sequence. In addition, Grymin et al. reframe the motion planning problem as a graph search, a common technique in robotics and motion planning, by constructing a graph of reachable states in an environment connected by primitives selected from a precomputed library.[7]

*Graduate Researcher, Colorado Center for Astrodynamics Research, Smead Department of Aerospace Engineering Sciences, University of Colorado Boulder, Boulder, CO 80303.

†Assistant Professor, Colorado Center for Astrodynamics Research, Smead Department of Aerospace Engineering Sciences, University of Colorado Boulder, Boulder, CO 80303.

Motivated by their application to robotics, Smith and Bosanac have applied the concept of motion primitives to trajectory design in a multi-body system. Specifically, we have formulated a consensus clustering procedure to numerically construct sets of motion primitives that summarize periodic orbit families and arcs along hyperbolic invariant manifolds based on geometry, stability, and energy in the Earth-Moon CR3BP.[2] We have then manually constructed sequences of motion primitives to produce coarse, primitive-based initial guesses that successfully enable recovery of nearby natural and maneuver-enabled transfers between libration point orbits in the Earth-Moon CR3BP.[3] This paper builds upon our previous work by using graph theory to guide the primitive-based initial guess construction process for trajectory design in a multi-body system with impulsive maneuvers.

The utility of graph-based searches in initial guess construction within astrodynamics has been demonstrated by a variety of researchers. Tsirogiannis explored a graph-based methodology for designing impulsive transfers between periodic orbits in the CR3BP using Dijkstra's algorithm.[8] Trumbauer and Villac developed an autonomous heuristic search-based framework for redesigning trajectories onboard a spacecraft in the CR3BP using precomputed dynamical structures, periapsis Poincaré maps, and the A* search algorithm.[9] Das-Stuart et al. construct an initial guess for a trajectory in the low-thrust enabled CR3BP using known dynamical structures, reinforcement learning, and Dijkstra's algorithm.[10] Furthermore, Parrish leveraged a graph-based approach for computing optimal continuous-thrust trajectories in the two-body problem using the A* search algorithm.[11] More recently, Bruchko and Bosanac have been using probabilistic roadmap generation and Dijkstra's algorithm to generate transfers between Lyapunov orbits in the CR3BP.[12] Although each of these contributions use distinct approaches for discretizing the solution space, they demonstrate the value of reframing the trajectory design problem as a discrete graph search problem.

This paper presents a generalized and modular graph structure of motion primitives that supplies a discrete representation of a design space to support constructing primitive-based initial guesses. First, sets of motion primitives and their associated regions of existence are constructed to summarize members of periodic orbit families and arcs along their hyperbolic invariant manifolds in the CR3BP.[2] Together, these sets form a motion primitive library. Subgraphs are then constructed to each reflect the relationships between the primitives summarizing a subset of dynamical structures: primitives form the nodes of the graph with edges connecting them to their k-nearest neighbors and weighted by their potential to produce a nearby continuous trajectory. These subgraphs are connected to form a motion primitive graph that may be customized to reflect complete or partial information about the itinerary of the desired trajectory. The motion primitive graph is then searched to produce distinct sequences of motion primitives that form initial guesses for transfers with distinct geometries. Continuous transfers are recovered from each initial guess using constrained optimization and collocation as presented by Smith and Bosanac and expanded in this paper.[3] This entire process is demonstrated by computing transfers of various geometries between periodic orbits near L_1 and L_2 in the Earth-Moon CR3BP. The result is a demonstration of the capability for an initial guess construction framework that uses motion primitives to rapidly generate candidate initial guesses for transfers of distinct geometries in cislunar space.

2 BACKGROUND

2.1 Dynamical Model

In this paper, the CR3BP is used to approximate the motion of a spacecraft for preliminary trajectory design in the Earth-Moon system. This dynamical system models the motion of a spacecraft of assumed negligible mass due to the gravitational influence of the Earth and the Moon, each modeled as point masses with masses M_1 and M_2, respectively, and traveling on circular orbits about their mutual barycenter.[1] A rotating reference frame is then defined using an origin at the barycenter of the system and axes $\{\hat{x}, \hat{y}, \hat{z}\}$: $\hat{x}$ is directed from the Earth to the Moon, $\hat{z}$ is aligned with the orbital angular momentum vector of the primary system, and $\hat{y}$ completes the right-handed triad.[1] In addition, quantities are often nondimensionalized using characteristic parameters for length (l^*), mass (m^*), and time (t^*): l^* is selected as the assumed constant distance between the Earth and Moon, m^* is equal to the total mass of the system, and t^* is calculated to produce a period of the primary system equal to 2π.[1,13] In the rotating frame, the nondimensional state of the spacecraft is then defined as $\bar{x} = [x, y, z, \dot{x}, \dot{y}, \dot{z}]^T$ and the resulting equations of motion are written as

$$\ddot{x} = 2\dot{y} + \frac{\partial U^*}{\partial x} \qquad \ddot{y} = -2\dot{x} + \frac{\partial U^*}{\partial y} \qquad \ddot{z} = \frac{\partial U^*}{\partial z} \tag{1}$$

where $U^* = 0.5(x^2+y^2) + (1-\mu)/r_1 + \mu/r_2$, $\mu = M_2/(M_1+M_2)$, $r_1 = \sqrt{(x+\mu)^2 + y^2 + z^2}$, and $r_2 = \sqrt{(x-1+\mu)^2 + y^2 + z^2}$. This autonomous dynamical system admits an integral of motion, the Jacobi constant, equal to

$$C_J = 2U^* - \dot{x}^2 - \dot{y}^2 - \dot{z}^2 \tag{2}$$

which is inversely proportional to the energy of the system. This quantity supplies insight into allowable regions of motion as well as heuristics for maneuver and trajectory design.[1,13]

2.2 Computing Fundamental Solutions

Natural solutions such as equilibrium points, periodic orbits, quasi-periodic orbits, and hyperbolic invariant manifolds typically serve as a basis for constructing complex trajectories in a chaotic multi-body gravitational environment. Thus, the presented framework focuses on extracting motion primitives that summarize natural fundamental solutions. This subsection offers a brief overview of computing periodic orbits and hyperbolic invariant manifolds in the CR3BP.

2.2.1 Periodic Orbits A periodic orbit is a trajectory that repeats after a minimal period in the rotating frame. These orbits and nearby bounded motions, if they exist, support identifying candidates for mission and staging orbits while also admitting hyperbolic invariant manifolds that influence natural transport. In the CR3BP, an infinite number of natural periodic orbits exist in the rotating frame in continuous families throughout the system.[1,13] In this paper, a single periodic orbit is computed numerically using a free variable and constraint vector formulation of multiple shooting and Newton's method.[13,14] First, an initial guess for a periodic orbit is computed using either Poincaré mapping, stability analysis, or resonance analysis techniques.[1,13–15] Then, this initial guess is discretized into a specified number of arcs of equal integration times. The states at the beginning of each arc, along with the common integration time, are assembled into the free variable vector. Next, a constraint vector is defined to enforce state continuity between each arc as well as periodicity. The free variable vector is iteratively updated from an initial guess using Newton's method until the magnitude of the constraint vector equals zero to within a tolerance of 10^{-12}, producing a numerical approximation of a periodic orbit in the CR3BP.[13,14] Pseudo-arclength continuation is then used to compute additional members along the family of periodic orbits.[14,16]

The local stability of a periodic orbit is used to characterize the behavior of the flow in the vicinity of the orbit. Motion in the vicinity of a periodic orbit may be bounded, exhibiting quasi-periodic motion, or unbounded, following hyperbolic invariant manifold structures. Stability indices, s_i, computed from the eigenvalues of the monodromy matrix associated with a state along a periodic orbit are often used to describe the local stability of the orbit.[17] Each stability index is defined as $s_i = \lambda_j + \lambda_k$, where λ_j and λ_k are eigenvalues of the monodromy matrix and form either a nontrivial reciprocal pair or complex conjugates. Using this definition, a stability index with a magnitude less than or equal to 2 indicates the presence of quasi-periodic motion while a magnitude greater than 2 indicates the presence of associated stable and unstable hyperbolic invariant manifolds.[13]

2.2.2 Hyperbolic Invariant Manifolds A trajectory along a stable manifold asymptotically approaches a periodic orbit in infinite time while a trajectory along an unstable manifold asymptotically departs from a periodic orbit.[13] In the absence of generalized analytical descriptions, an approximation of a stable or unstable manifold is computed numerically. First, an unstable periodic orbit is discretized into a set of states. At each state, a perturbation is applied in the direction of the stable (or unstable) eigenvector of the associated monodromy matrix.[13] Then, the perturbed state is propagated backward (or forward) in time to produce a trajectory along the global stable (or unstable) manifold. This numerical process is repeated for each state along the periodic orbit to produce a discrete approximation of the desired manifold. In finite time, trajectories that lie along these approximations of global hyperbolic invariant manifolds support the design of transfers between periodic orbits and/or distinct regions of cislunar space.

2.3 Numerically Correcting Trajectories

Collocation is an implicit integration method that is often used in differential correction algorithms to compute a continuous trajectory from an initial sequence of discontinuous trajectory segments.[18] The collocation implementation used in this paper follows the formulation of a generalized odd-degree collocation scheme with hybrid mesh refinement presented by Grebow and Pavlak.[19] Given an initial sequence of trajectory segments, a discrete mesh of nodes is first defined by discretizing each trajectory segment into a series of arcs. The nodes at the boundaries of each arc are denoted as boundary nodes. Then, collocation nodes are defined along each arc within each segment based on a desired node spacing strategy. Within a given arc, the odd-numbered nodes are classified as free nodes and the even-numbered nodes are classified as defect nodes. The motion along each arc is then approximated using a set of polynomials constructed from the states at each free node. Each polynomial is a function of time and approximates the evolution of a single state along the given arc. Coupled with continuity constraints between trajectory segments, a trajectory is then computed by iteratively adjusting the free nodes along each arc until the resulting sets of piecewise polynomials satisfy the equations of motion for the dynamical system at the defect nodes. Based on previous applications of collocation for numerically correcting trajectories in multi-body systems, 7th order polynomials are used for approximating the dynamics and Legendre-Gauss-Lobatto (LGL) nodes are used to place the collocation nodes along each arc.[19–22] Leveraging collocation and mesh refinement in a differential correction algorithm, as demonstrated in Smith and Bosanac, enables robust recovery of continuous natural and maneuver-enabled transfers that geometrically resemble a coarsely constructed primitive-based initial guess.[3]

3 PRIMITIVE-BASED TRANSFER DESIGN PROCESS

In this section, a primitive-based initial guess construction framework is formulated to rapidly generate trajectories in multi-body systems. This procedure consists of the following steps:

1. Construct a motion primitive library.
2. Construct a motion primitive graph that discretely approximates the solution space.

3. Search the graph for motion primitive sequences that serve as candidates for initial guesses.
4. Construct an initial guess for a trajectory by refining a motion primitive sequence.
5. Correct the initial guess to produce a trajectory using direct collocation and optimization.

This section demonstrates each step of the initial guess construction process using a foundational example of a transfer from an L_1 to L_2 Lyapunov orbit in the Earth-Moon CR3BP.

3.1 Step 1: Construct a Motion Primitive Library

The first step in the initial guess construction framework is to construct a library of motion primitives and their regions of existence using the process previously presented by Smith and Bosanac.[2] Although the definition of a motion primitive depends on the application, we use a similar definition to Frazzoli: a set of motion primitives is a finite set of arcs that sufficiently summarize the characteristics of the solution space.[2,23] Based on this definition, a motion primitive library supplies a discrete summary of part of the solution space. Consequently, an initial guess for a trajectory may be coarsely constructed from an ordered sequence of motion primitives within the library.[4,5,23]

In our proof of concept, we have previously defined and computed motion primitives for trajectory design that summarize periodic orbits and arcs along hyperbolic invariant manifolds in the CR3BP.[2] To compute these motion primitives, we have previously developed a clustering-based approach.[2] First, a set of continuous trajectories are described using a finite but high-dimensional feature vector that reflects their geometric, stability, and/or energetic properties. For each trajectory, the geometric component of the feature vector, $\bar{f}_g$, is defined using the sequence of states at each of the l apses along the trajectory with respect to a specified reference point as

$$\bar{f}_g = \begin{bmatrix} \tilde{x}_1 & \tilde{y}_1 & \tilde{z}_1 & \dot{\tilde{x}}_1 & \dot{\tilde{y}}_1 & \dot{\tilde{z}}_1 & \cdots & \tilde{x}_l & \tilde{y}_l & \tilde{z}_l & \dot{\tilde{x}}_l & \dot{\tilde{y}}_l & \dot{\tilde{z}}_l \end{bmatrix} \tag{3}$$

where the tilde indicates normalization of each feature within the range $[-1, 1]$. For periodic orbits, the stability component of the feature vector uses the stability indices as

$$\bar{f}_s = \left[\tanh\left(\frac{s_1}{2}\right) \quad \tanh\left(\frac{s_2}{2}\right)\right] \tag{4}$$

and the energy component, f_e, is calculated using the Jacobi constant of the orbit as

$$f_e = \tilde{C}_J \tag{5}$$

Using these definitions, the feature vector for a periodic orbit is defined as

$$\bar{f}_{PO} = \begin{bmatrix} \bar{f}_g & \bar{f}_s & f_e \end{bmatrix} \tag{6}$$

with a length of $6l_{\max} + 3$ where $l_{\max}$ is the maximum number of apses along all trajectories in the set. The feature vector for an arc along a stable or unstable manifold is defined as

$$\bar{f}_{Mani} = \begin{bmatrix} \bar{f}_g & \Delta\tilde{t}_1 & \cdots & \Delta\tilde{t}_{l-1} \end{bmatrix} \tag{7}$$

where $\Delta\tilde{t}_i$ is the time between the i-th and $(i+1)$-th apses, normalized by the integration time of the arc, and $\bar{f}_{Mani}$ possesses a length of $7l_{\max} - 1$. Then, Weighted Evidence Accumulation Clustering (WEAC) is applied to the feature vectors of the trajectory set to identify clusters of trajectories with similar properties; for more details about this process, see Smith and Bosanac 2022.[2] A motion primitive is extracted from each of these clusters as its medoid, i.e., the most similar member to all other members in the cluster.[24] The resulting motion primitive set and their corresponding clusters produce a discrete summary of the types of motion present across the given set of trajectories.

The region within the phase space that produces trajectories resembling a motion primitive depends on the properties of the system as well as the definition of the primitive itself. In robotics, a motion primitive is commonly defined as a type of control input or fundamental type of action a robot may take to move anywhere within its environment unless hindered by a hardware or operational constraint.[23,25,26] However, trajectories in the chaotic environment of the CR3BP that resemble a specific motion primitive, given the specific definition used by Smith and Bosanac, only exist within a particular region of the phase space. In our previous work, we label this the 'region of existence' of the motion primitive;[3] conceptually similar to a funnel used to describe controlled trajectories in the vicinity of a primitive.[27] In our previous work, the use of clustering to construct a motion primitive directly supplies an approximation of its region of existence as the region of the phase space spanned by the corresponding cluster. To limit data storage complexity for this information, a finite number of representative trajectories are identified from each cluster using k-means clustering.[3] Then, the region of existence associated with a motion primitive is approximated using the set $R_E = \{\bar{x}_R(t) \in C\}$, where $\bar{x}_R(t)$ is one of a finite number of representative trajectories extracted from cluster C corresponding to the primitive. Using this region of existence associated with a motion primitive in the trajectory design process may significantly improve the quality of a coarse preliminary primitive-based initial guess.

To demonstrate this step of the design process, consider sets of motion primitives that support the construction of a planar transfer from an L_1 Lyapunov orbit to an L_2 Lyapunov orbit in the Earth-Moon CR3BP. The selected L_1 Lyapunov orbit exists at $C_J = 3.1670$ whereas the selected L_2 Lyapunov orbit exists at $C_J = 3.1666$; both of these orbits are primitives of their associated periodic orbit families and both possess stable/unstable manifolds. Then, primitive sets describing arcs along stable and unstable half-manifolds of the selected L_1 and L_2 Lyapunov orbits are generated. Table 1 lists the resulting properties for each primitive set. Furthermore, Figure 1 displays the initial L_1 Lyapunov orbit primitive, the target L_2 Lyapunov orbit primitive, and selected motion primitives from their stable and unstable manifolds. Each primitive is denoted in bold and its associated region of existence is depicted as a surface generated from the discrete set of representative trajectories. These primitive sets form a condensed primitive library for the example design scenario.

Table 1. Motion primitives in the library for the L_1 to L_2 Lyapunov orbit transfer scenario.

Fundamental Solution	Number of Primitives	C_J	Manifold Generation Properties
L_1 Lyapunov orbit	1	3.1670	-
L_1 Lyapunov orbit unstable manifold	45	3.1670	Max. of 15 apses wrt Moon
L_1 Lyapunov orbit stable manifold	34	3.1670	Max. of 6 apses wrt Moon
L_2 Lyapunov orbit	1	3.1666	-
L_2 Lyapunov orbit unstable manifold	33	3.1666	Max. of 6 apses wrt Moon
L_2 Lyapunov orbit stable manifold	65	3.1666	Max. of 15 apses wrt Moon

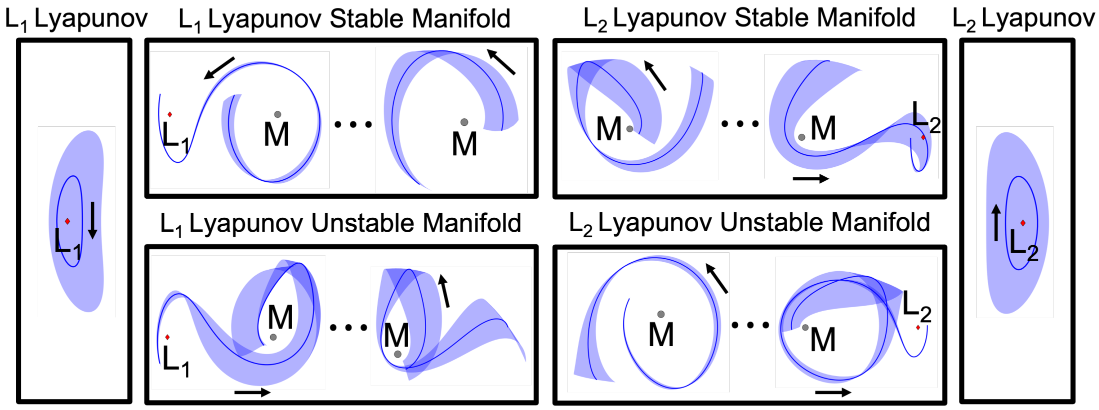

Figure 1. Examples of motion primitives (bold) and their associated regions of existence from the motion primitive library for the L_1 to L_2 Lyapunov orbit transfer scenario in the Earth-Moon system.

3.2 Step 2: Construct a Motion Primitive Graph

The next step of the design process is to construct a motion primitive graph that produces a discrete representation of regions of the continuous solution space in a multi-body system. In general, a graph is a discrete data structure composed of a set of nodes and edges that is often used to model the properties and internal relationships of a network of objects.[5,28] In this paper, each motion primitive and its corresponding region of existence is a node in the graph. Then, a set of weighted, directed edges reflects the potential for selected pairs of primitives to be composed in a sequence to produce a nearby continuous trajectory with similar geometric properties. Using this application of graph theory, the trajectory design problem is reframed as a discrete graph search problem. However, to incorporate designer expertise and reduce computational complexity, the graph construction process is composed of two steps in this paper: (1) constructing subgraphs reflecting the relationships between motion primitives associated with a single type of dynamical structure and (2) constructing a modular, high-level itinerary graph to connect these subgraphs.

Formulating a motion primitive graph requires determining the sequential composability of an ordered pair of primitives; a property that is described by Majumdar and Tedrake as their potential to produce a nearby trajectory.[27] In funnel libraries, this property is straightforwardly calculated by identifying overlapping funnels. However, to avoid overfitting to an incomplete approximation of a region of existence, we estimate the potential for sequential composability of two motion primitives $\bar{x}_{P,i}$ and $\bar{x}_{P,j}$ and, potentially, their regions of existence $R_{E,i}$ and $R_{E,j}$ using the following metric:

$$q = \alpha_{Pos}\Delta r + \alpha_{Vel}\Delta v \tag{8}$$

where Δr, Δv are the magnitudes of the position and velocity difference, respectively, between two primitives and, potentially, their regions of existence. In addition, α_{Pos}, α_{Vel} scale the position and velocity differences, respectively. With this definition, a lower value of q corresponds to a higher potential for two sequentially composed motion primitives to produce a nearby continuous path.

To evaluate the potential for sequential composability of two motion primitives, the state difference between trajectories must be calculated. First, each trajectory is discretized into a sequence of states: in this paper, each periodic orbit primitive is discretized into 25 states equally spaced in arclength and each manifold arc primitive is discretized into apses with respect to the Moon. Then, the state difference between two trajectories is calculated using one of the following four metrics:

1. the difference between the final state of the first trajectory and the initial state of the second trajectory
2. the minimum difference between any state along the first trajectory and the initial state of the second trajectory
3. the minimum difference between the final state of the first trajectory and any state along the second trajectory
4. the minimum difference between any state along the first trajectory and any state along the second trajectory

Figure 2 supplies a conceptual depiction of each of these state difference definitions; note that the last three definitions enable identification of two trajectories with closely located segments that could produce a nearby, continuous path. To evaluate Equation 8, the state difference may be calculated using only the primitives or both the primitives and the representative trajectories spanning their associated regions of existence. If the regions of existence are used, the state difference is calculated as the minimum state difference between any representative trajectory from the first region of existence and any representative trajectory from the second region of existence.

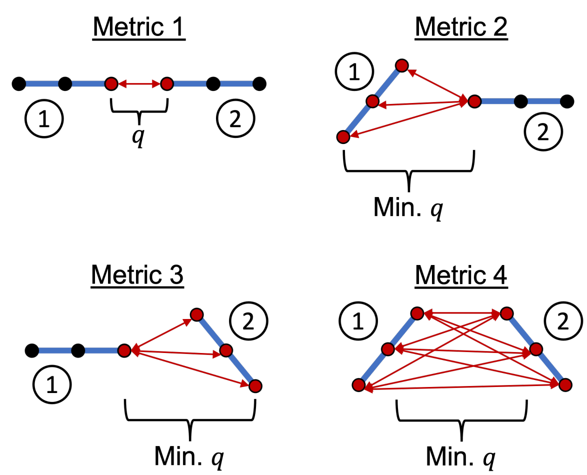

Figure 2. Methods for computing the state difference between an ordered pair of trajectories.

Using the potential for sequential composability, a subgraph of each motion primitive set is formed. With motion primitives at each node of a subgraph, weighted and directed edges are added to the k-nearest neighbors of each node where $k \geq 0$. If $k = 0$, the subgraph has no internal edges and therefore primitives within the subgraph may not be sequentially composed. However, for $k > 0$, the neighbors for each primitive are identified using the k lowest values of q for each possible ordered primitive pair, calculated using Metric 1 between the primitives and, if desired, their regions of existence. The edge weights are then assigned as the sequential composability, q, for each connected pair of primitives. A conceptual representation of a subgraph is depicted in Figure 3a) where each black circle is a node in the graph and is connected to its three nearest neighbors in the set ($k = 3$). As a result, the subgraph reflects the potential for an ordered sequence of two primitives in the set to be useful in the initial guess construction process.

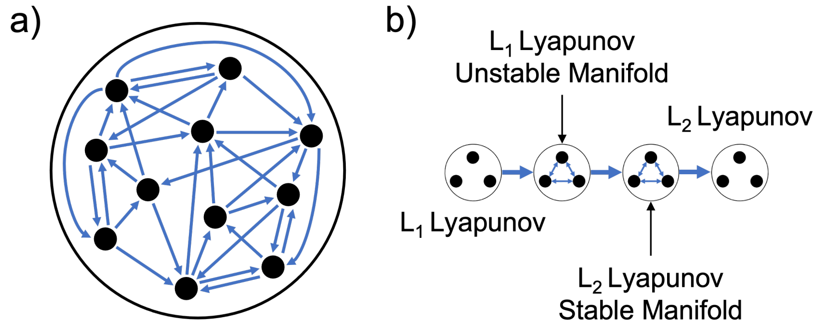

Figure 3. a) Conceptual representation of a subgraph and b) a high-level itinerary graph design for the L_1 to L_2 Lyapunov orbit transfer scenario in the Earth-Moon CR3BP.

The subgraphs are then connected according to a modular high-level itinerary graph that is constructed by the trajectory designer. In particular, the designer specifies any external connections, i.e. directed edges, between the subgraphs that each capture members of a primitive set associated with a single dynamical structure. This step enables the designer to incorporate their expertise, or even lack thereof, in a scenario into the structure of the graph. To construct the external connections between subgraphs, each individual primitive in the source subgraph is connected to its k-nearest neighbors in the target subgraph via directed edges. However, there is one exception: if the target subgraph only contains the final target orbit then only the edges between the final target orbit and its k-nearest neighbors in the source subgraph are created. Similar to the subgraph construction process, the external edge weights are assigned as the potential sequential composability between each connected pair of primitives: Metric 2 is used to compute q if the source primitive is a periodic orbit and the target primitive is a manifold arc but otherwise Metric 3 is used. As a result of this process, the value of k determines the degree of connectivity in the full motion primitive graph.

To demonstrate the presented approach, consider a high-level itinerary graph constructed using select primitive sets from the library in Table 1 for the L_1 to L_2 Lyapunov orbit transfer example. A conceptual representation of this graph appears in Figure 3b). In this figure, the arrows within the icon associated with an unstable manifold of the initial L_1 Lyapunov orbit indicate that the nodes of the subgraph are connected by internal edges, thereby allowing multiple primitives from the unstable manifold set to be sequentially composed in an initial guess. In contrast, the icon for the L_1 Lyapunov orbit denotes a subgraph with no internal edges, indicating there is no potential for sequential composability within the set. The unidirectional arrows between subgraphs then indicate a desired order for composing primitives from each set. This high-level itinerary graph indicates that an initial guess may only be composed of the following primitives in the specified order: one primitive from the L_1 Lyapunov orbit family set, one or more primitives from the unstable half-manifold of the selected L_1 Lyapunov orbit, one or more primitives from the stable half-manifold of the selected L_2 Lyapunov orbit, and one primitive from the L_2 Lyapunov orbit family set. If these arrows were bidirectional, then primitives from each subgraph could be composed in any order, consistent with the designer either having less insight into the transfer geometry or considering a wider variety of solution itineraries.

For the L_1 to L_2 Lyapunov orbit transfer example, a motion primitive graph is constructed using the high-level itinerary graph in Figure 3b) and the corresponding primitive sets from the library in Table 1. The primitives within each manifold subgraph are connected internally with their $k = 20$ nearest neighbors as well as externally to their $k = 20$ nearest neighbors in their connected subgraphs. The resulting motion primitive graph is displayed in Figure 4a); each node in the graph is depicted as a black dot, the internal edges within the L_1 Lyapunov unstable manifold subgraph are denoted in red, the internal edges within the L_2 Lyapunov stable manifold subgraph are denoted in light blue, and all external edges between nodes in different subgraphs are depicted with dark blue arrows. This motion primitive graph is used to construct coarse, primitive-based initial guesses.

3.3 Step 3: Identify Candidate Motion Primitive Sequences

The motion primitive graph is searched to produce a primitive sequence that supports constructing a coarse primitive-based initial guess for a trajectory. There are many different graph search techniques that may be used to find and evaluate a path from an initial node to a target node. In this preliminary proof of concept, the common brute-force search algorithm, depth-first search (DFS), is used to enumerate all potential paths in a motion primitive graph from an initial node to a target node with a desired length.[5] The sequence length is defined as the number of primitives chained together in a single sequence. Each path identified using DFS corresponds to a discontinuous sequence of motion primitives. The quality of each candidate primitive sequence in predicting a nearby continuous trajectory is then captured by either the average or maximum edge weight along the path as determined by the trajectory designer. The candidate sequences are then ranked based on their quality and only a desired number of the best ranked sequences are considered. A trajectory designer may then identify distinct primitive sequences to refine and use to construct initial guesses.

To demonstrate this step in the context of the L_1 to L_2 Lyapunov orbit transfer example in the Earth-Moon system, the top-ranked 25 primitives sequences consisting of four primitives with the lowest average edge weight are generated from the motion primitive graph displayed in Figure 4a). None of these candidate sequences are guaranteed to predict nearby continuous trajectories with similar geometric properties. However, a trajectory designer may examine each primitive sequence and average values of q to determine whether to perform further analysis and refinement. As an example, the primitive sequence with the lowest average value of q admits a single revolution around the Moon. This primitive sequence is identified in the motion primitive graph in Figure 4a) and is plotted in the Earth-Moon rotating frame in Figure 4b). Each primitive is denoted in bold with a distinct color in Figure 4b) whereas the associated region of existence is plotted in the same color as a surface generated from the discrete set of representative trajectories. Furthermore, the initial (final) state of each primitive is denoted with a filled (empty) circle. Although this example presents only the top-ranked sequence of four motion primitives, it supports demonstrating the coarse construction of an initial guess for a transfer using motion primitives. Additional primitive sequences for this design scenario are explored in Section 4.1.

3.4 Step 4: Construct an Initial Guess from a Primitive Sequence

A candidate motion primitive sequence is refined to improve the quality of a coarsely-constructed initial guess and facilitate better convergence behavior during the numerical corrections process. The primitive sequence displayed in Figure 4b) possesses small state discontinuities between each consecutive pair of primitives and exhibits a significant overlap between the second and third primitives in the sequence. Consequently, the first step in refining an initial guess is to trim each arc to remove any overlapping portions. The trimming process is completed automatically by trimming each primitive and its region of existence to start (or end) at their closest state in the phase space

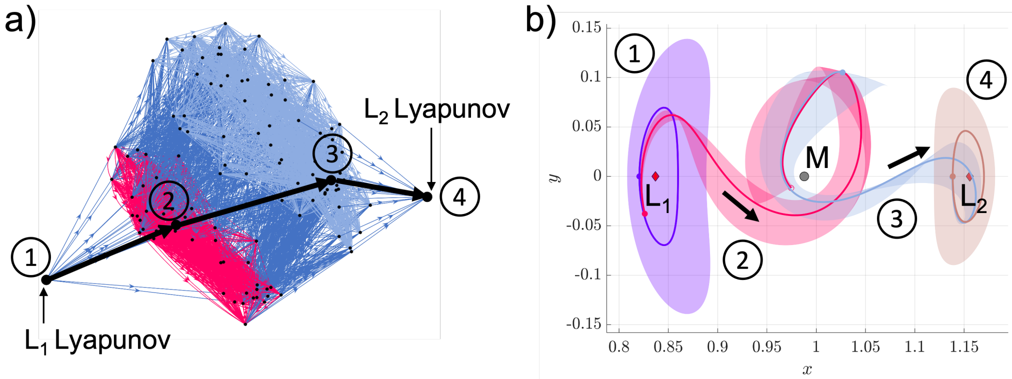

Figure 4. A motion primitive sequence for a transfer between an L_1 and L_2 Lyapunov orbit in the Earth-Moon system displayed in a) the motion primitive graph for the design scenario and b) the rotating frame of the Earth-Moon CR3BP.

relative to the final (or initial) state of the previous (or next) primitive in the sequence.

The second refinement step is to morph the trimmed primitives within their regions of existence to further reduce the state discontinuities along the initial guess. Recall that the region of existence associated with each motion primitive is approximated by a finite set of representative trajectories; using one of these representative trajectories may produce a better initial guess than using the primitive. Thus, all possible candidate initial guesses with similar geometry to the original motion primitive sequence are constructed by using either each motion primitive or one of the representative trajectories spanning its region of existence. The average value of the potential sequential composability (as defined in Section 3.2 as the quantity q) along each candidate sequence of arcs is computed: Metric 2 is used to measure the state difference between a periodic orbit followed by a manifold trajectory; Metric 1 is used to measure the state difference between each pair of manifold trajectories because the interior primitives and their regions of existence have been trimmed; and Metric 3 is used to measure the state difference between a manifold trajectory followed by a periodic orbit. The sequence of arcs with the smallest average value of the sequential composability metric q produces the morphed initial guess that is used for further analysis.

Using the outlined process, the primitive sequence depicted in Figure 4b) is trimmed and morphed. Figure 5 displays the original initial guess in dashed gray after the trimming process is complete. Through this process, the overlap between the second and third primitives is removed. Figure 5 also displays the morphed initial guess in blue. The initial guess selected in this example already exhibited small state discontinuities before being morphed within its associated regions of existence. However, morphing the initial guess within its associated regions of existence improved the quality of the initial guess by further reducing the state discontinuity between the second and third arcs in the sensitive region of the phase space near the Moon.

3.5 Step 5: Recover a Continuous, Optimal Trajectory

The final step is to compute a continuous trajectory that resembles the primitive-based initial guess. To implement this step, the goal of the corrections process is to minimize the dissimilarities between the final continuous trajectory and the initial guess. In robotic motion planning as well as periodic orbit computation in multi-body systems, constrained optimization methods have previously been used to compute trajectories with similar geometries as a reference path.[14,29] However,

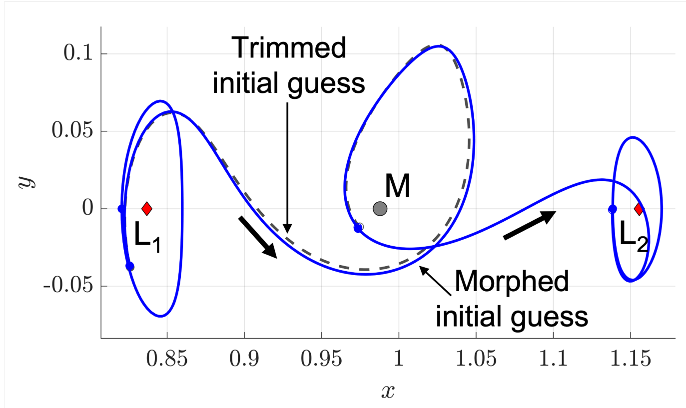

Figure 5. Refined primitive-based initial guess for a transfer between an L_1 and L_2 Lyapunov orbit in the Earth-Moon CR3BP.

computing a geometrically similar solution to an initial guess may not be the only design objective for a mission scenario. Maneuver magnitudes are also often a primary concern in the trajectory design process. Thus, a multi-objective constrained optimization problem is formulated.

An objective function is formulated to include both the difference in geometry between two trajectories and the cumulative maneuver requirements. This objective function is defined as

$$J(\bar{V}) = w_{Geo}((\bar{V}_{Pos} - \bar{V}_{IG_{Pos}})^T(\bar{V}_{Pos} - \bar{V}_{IG_{Pos}})) + w_{Man}\left(\sum_{i=1}^{M} \Delta v_i^2\right) \tag{9}$$

where $\bar{V}_{Pos}$ and $\bar{V}_{IG_{Pos}}$ reflect only the position components of the free variable vector $\bar{V}$ during the current iteration and the initial guess, respectively; w_{Geo} and w_{Man} are the relative weights of the geometric and maneuver terms, respectively; Δv_i is the magnitude of the i-th maneuver; and M is the number of maneuvers.

An overview of the corrections procedure formulated to compute a maneuver-efficient trajectory that geometrically resembles a primitive-based initial guess is depicted in Figure 6. First, a primitive-based initial guess is constructed, such as the initial guess displayed in Figure 5 for the L_1 to L_2 Lyapunov orbit transfer example, and a corrections scheme is defined. For transfers between two periodic orbits, the periodic orbit primitives are removed from the initial guess and the corrections scheme is formulated such that the transfer is constrained to depart from the desired initial orbit primitive and arrive onto the desired target orbit primitive. Using the collocation approach outlined in Section 2.3, each segment of the initial guess is discretized into a series of arcs with equal arclength. Then, 7th order polynomials and LGL nodes are used to place collocation nodes along each arc and formulate both the continuity and collocation constraints for the constrained optimization problem. The free nodes and Δt of each arc along the initial guess comprise the free variable vector; however, two additional free variables, Δt_{Depart} and $\Delta t_{Arrival}$, measured from specified states along the initial and final orbits, are included to allow the departure and arrival locations to vary. In addition, impulsive maneuvers are allowed at the beginning and end of the transfer to depart from the initial orbit and arrive onto the target orbit. When desired, impulsive maneuvers are also placed between each pair of primitives. For each maneuver, velocity continuity constraints between the associated arcs are removed. The open source Interior Point OPTimizer (IPOPT) software library is then used to solve this problem while minimizing the objective function given an initial

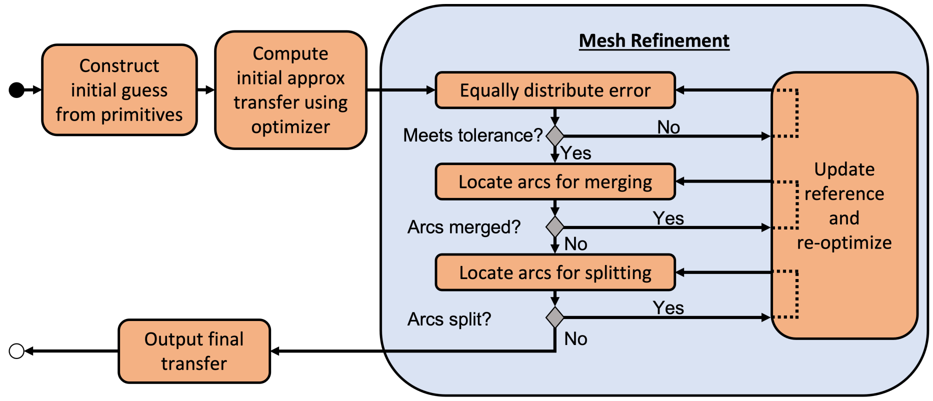

Figure 6. Conceptual overview of the corrections algorithm used to compute a maneuver-efficient trajectory that resembles a primitive-based initial guess.[3]

guess.[30] However, the resulting solution must be refined to ensure numerical accuracy.

The numerical accuracy of a trajectory computed using collocation depends on the quality of the node mesh used to discretize the solution and approximate the dynamics of the system. Consequently, the hybrid mesh refinement procedure presented by Grebow and Pavlak is used to refine the initial approximate solution.[19] As depicted in Figure 6, this process involves sequentially distributing error along the solution, removing any unnecessary arcs to reduce the size of the parameter optimization problem, and adding arcs to the mesh to ensure the solution is numerically accurate. During each iteration of the mesh refinement process, the reference initial guess that is passed into IPOPT is the last converged solution. The final output of the algorithm is a continuous trajectory that minimizes maneuver requirements while resembling the initial guess.

The numerical corrections procedure summarized in Figure 6 is applied to the initial guess constructed for the L_1 to L_2 Lyapunov orbit transfer example. Values of $w_{Geo} = 0.9$ and $w_{Man} = 0.1$ in the objective function in Equation 9 are selected to prioritize maintaining the transfer geometry of the initial guess while building in some flexibility to recover a maneuver-efficient solution. Of course, these weights may be adjusted to prioritize a different balance of the objectives. Following optimization, the resulting continuous trajectory is displayed in Figure 7 with the morphed initial guess displayed in dashed gray, the initial and target periodic orbits displayed in solid gray, and the final continuous solution displayed in solid blue. This transfer includes a departure maneuver of $5.3\ m/s$, an arrival maneuver of $1.6\ m/s$, and a time-of-flight (TOF) equal to 23.5 days. This trajectory closely resembles the morphed initial guess due to the high quality of the initial guess and objective function formulation. Despite the simplicity of this example, it demonstrates the procedure for using motion primitives to coarsely construct an initial guess with a desired transfer geometry and generate a nearby continuous trajectory.

4 RESULTS: PRIMITIVE-BASED TRANSFER DESIGN SPACE EXPLORATION

The primitive-based initial guess construction framework presented in Section 3 enables rapid generation of trajectories with distinct geometries in a multi-body system. This section demonstrates the use of the framework to generate a variety of transfers between libration point orbits in the Earth-Moon system. The design space is explored for transfers between selected L_1 and L_2 Lyapunov orbits as well as between selected L_1 and L_2 northern halo orbits.

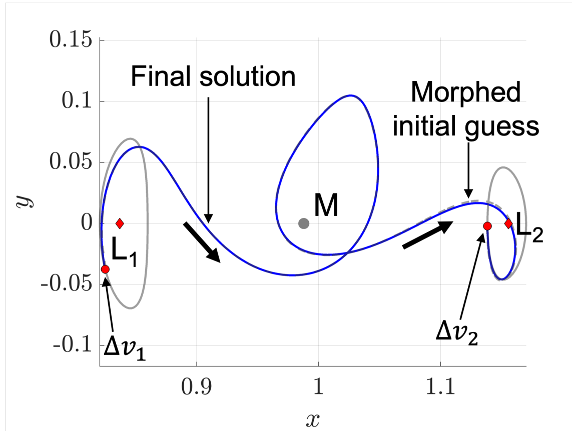

Figure 7. Continuous 23.5 day transfer between an L_1 and L_2 Lyapunov orbit in the Earth-Moon CR3BP computed from a primitive-based initial guess.

4.1 L_1 to L_2 Lyapunov Orbit Transfers

In this subsection, transfers are constructed between an L_1 and L_2 Lyapunov orbit in the Earth-Moon system. Recall that in Section 3, the example used to demonstrate the initial guess construction process also involves a transfer from an L_1 to L_2 Lyapunov orbit. However, the itinerary graph developed in Section 3 assumes the designer possesses a priori knowledge of the design space and itinerary of trajectories. However, now assuming that the designer does not possess this a priori knowledge, a more general motion primitive graph is constructed using all of the primitives in the sets listed in Table 1. The associated high-level itinerary graph is depicted in Figure 8 with a more general structure than in Figure 3b). To construct the resulting motion primitive graph, the following configuration parameters are specified: $\alpha_{Pos} = 10$, $\alpha_{Vel} = 1$, and $k = 10$. Additionally, the region of existence of each motion primitive is incorporated into the edge weight computations and the average edge weight is used to evaluate the quality of each primitive sequence. Equipped with the full motion primitive graph for this design scenario, a variety of transfers are constructed.

Initial guesses are constructed using four-primitive sequences that are identified from the more general motion primitive graph for the L_1 to L_2 Lyapunov orbit transfer design scenario. A total

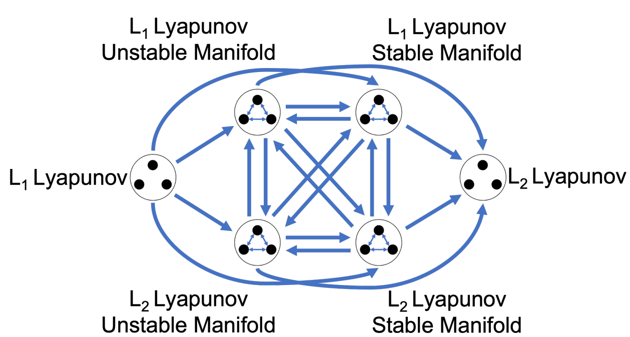

Figure 8. High-level itinerary graph for an L_1 to L_2 Lyapunov orbit transfer design scenario in the Earth-Moon system developed assuming the human designer has minimal a priori knowledge of the design space.

of 25 four-primitive sequences are identified. However, Figure 9 displays four distinct, continuous transfers (solid blue) computed using $w_{Geo} = 0.9$ and $w_{Man} = 0.1$ from the top-ranked primitive sequences. The morphed initial guess for each transfer is displayed in dashed gray and the initial and target orbit primitives are displayed in solid gray. Each transfer contains three impulsive maneuvers, each located between neighboring arcs from the initial guess. The associated maneuver magnitudes and transfer times are summarized in Table 2. Transfer Lyap-4P1, the best ranked primitive sequence, uses the same primitives as the example presented in Section 3; this result demonstrates the capacity to recover similar, straightforward solutions when little a priori knowledge is incorporated into the graph construction process. In addition, Lyap-4P1 and Lyap-4P2 resemble heteroclinic connections between L_1 and L_2 Lyapunov orbits at nearby energy levels. Finally, Lyap-4P1, Lyap-4P2, Lyap-4P3, and Lyap-4P4 each exhibit distinct geometries and revolutions around the Moon, consistent with each transfer being constructed from distinct four-primitive sequences.

Five- and six-primitive sequences that connect the initial and final L_1 and L_2 Lyapunov orbits are also constructed from the motion primitive graph. The transfers computed using $w_{Geo} = 0.9$ and $w_{Man} = 0.1$ from a few of the top-ranked primitive sequences (amongst 25 candidates for five- and six-primitive sequences, respectively) are displayed in Figure 10. Their maneuver magnitudes and transfer times are also summarized in Table 2. In these figures, the transfers constructed from sequences of additional primitives generally exhibit more complex geometries but contain some common elements with the transfers constructed from fewer primitives. However, Lyap-5P3 in Figure 10 resembles Lyap-4P2 in Figure 9 due to the same transfer geometry being described by a slightly different sequence of motion primitives. In each case, the transfers geometrically resemble their corresponding initial guesses. As a result, they demonstrate the utility of the primitive-based initial guess construction framework in rapidly examining the transfer design space.

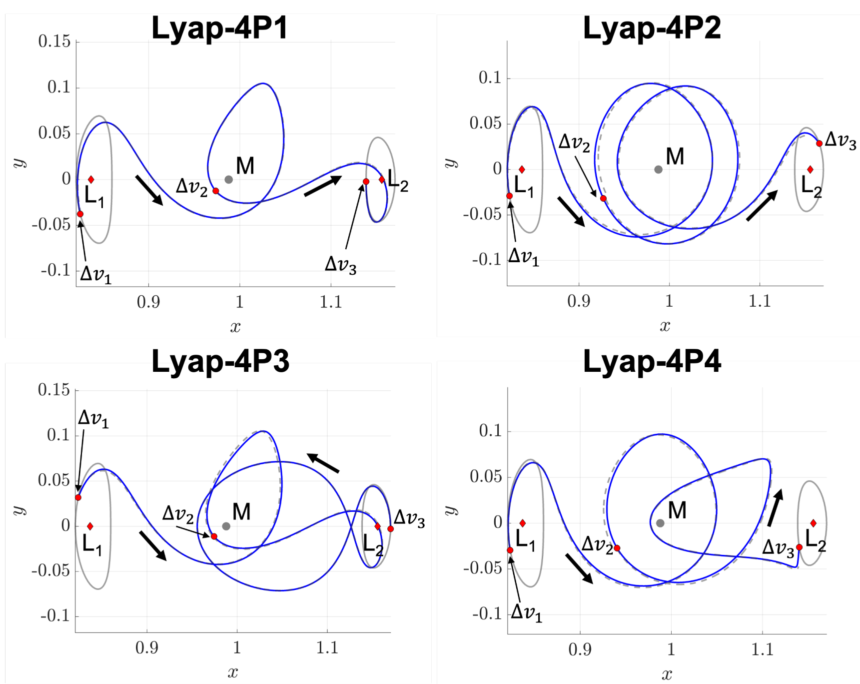

Figure 9. Transfers with distinct geometries between an L_1 and L_2 Lyapunov orbit in the Earth-Moon CR3BP computed from four-primitive initial guesses.

Table 2. Maneuver magnitudes and time-of-flight (TOF) between the L_1 and L_2 Lyapunov orbits.

Transfer Name	Δv_1 $[m/s]$	Δv_2 $[m/s]$	Δv_3 $[m/s]$	Δv_4 $[m/s]$	Δv_5 $[m/s]$	Total Δv $[m/s]$	TOF [days]
Lyap-4P1	5.4	0.8	1.2	-	-	7.4	23.5
Lyap-4P2	4.2	17.6	16.7	-	-	38.5	29.0
Lyap-4P3	22.0	3.5	1.9	-	-	27.4	37.4
Lyap-4P4	2.9	8.6	21.1	-	-	32.6	28.0
Lyap-5P1	4.6	28.7	89.1	5.0	-	127.4	37.2
Lyap-5P2	2.8	1.7	12.4	2.7	-	19.6	45.2
Lyap-5P3	2.1	3.8	3.7	4.4	-	14.0	30.9
Lyap-6P1	9.1	34.6	82.6	7.7	3.0	137.0	43.2
Lyap-6P2	2.0	1.3	0.7	0.6	4.1	8.7	38.3

4.2 L_1 to L_2 Northern Halo Orbit Transfers

In this subsection, the primitive-based initial guess construction framework is used to construct spatial transfers between an L_1 and L_2 northern halo orbit in the Earth-Moon CR3BP. In this scenario, Poincaré maps capturing spatial arcs along stable or unstable manifolds or within the general solution space may be difficult to analyze. As a result, it may be challenging to use existing dynamical systems techniques alone to both construct point solutions and explore the broader design space spanned by geometrically dissimilar solutions. For this design scenario, the high-level itinerary graph design matches the structure from Figure 3b) used for the example in Section 3. Table 3 lists the primitive sets from the motion primitive library that are used to construct the motion primitive graph and the following configuration parameters are specified: $\alpha_{Pos} = 10$, $\alpha_{Vel} = 1$, and $k = 15$. Additionally, the region of existence associated with each motion primitive is incorporated into the edge weight computations and the maximum edge weight is used to evaluate the quality of each primitive sequence. Using this motion primitive graph, a variety of transfers are constructed.

Transfers derived from sequences of four and five primitives are constructed from the L_1 to L_2 northern halo orbits. Figure 11 displays four distinct transfers computed using $w_{Geo} = 0.9$ and

Table 3. Motion primitives in the library for the L_1 to L_2 northern halo orbit transfer scenario.

Fundamental Solution	Number of Primitives	C_J	Manifold Generation Properties
L_1 northern halo orbit	1	3.0635	-
L_1 northern halo orbit unstable manifold	79	3.0635	Max. of 15 apses wrt Moon
L_2 northern halo orbit	1	3.0669	-
L_2 northern halo orbit stable manifold	94	3.0669	Max. of 15 apses wrt Moon

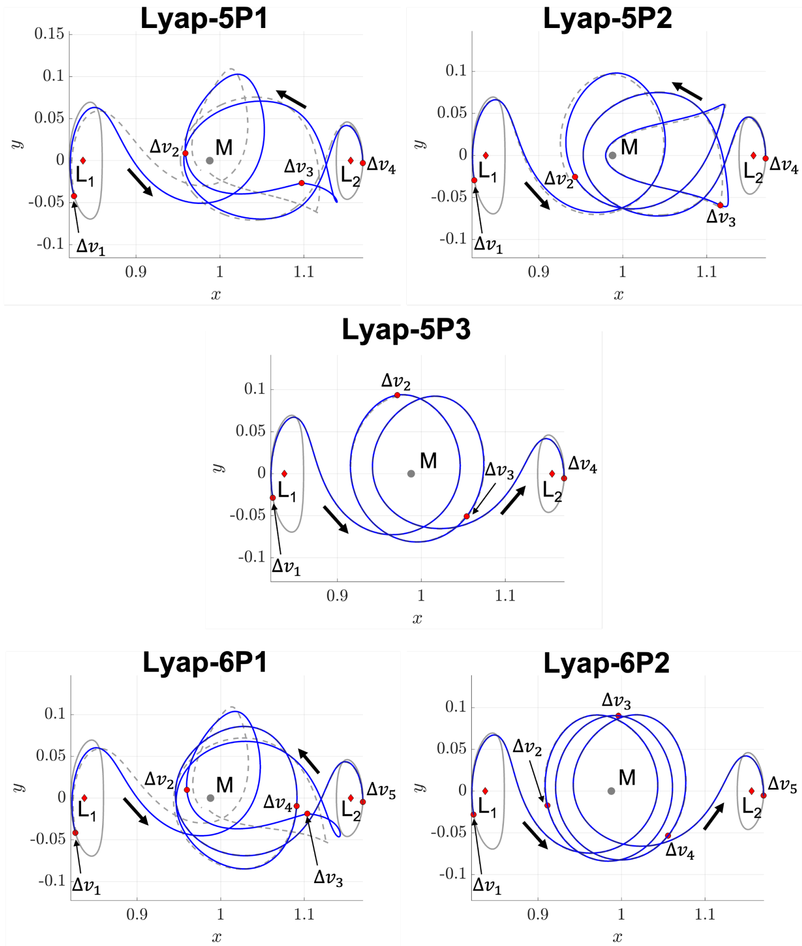

Figure 10. Transfers with distinct geometries between an L_1 and L_2 Lyapunov orbit in the Earth-Moon CR3BP computed from five- and six-primitive initial guesses.

$w_{Man} = 0.1$ from the top-ranked four- and five-primitive sequences (amongst 25 candidates each respectively). The maneuver magnitudes and transfer times for each transfer presented in Figure 11 are summarized in Table 4. In Figure 11, each trajectory (solid blue) closely retains the geometry of its initial guess (dashed gray). NHalo-4P, NHalo-5P1, and NHalo-5P2 all exhibit distinct transfer geometries in the vicinity of the Moon with several close approaches below the plane of the primaries and apolunes at high z-amplitudes above the plane of the primaries. Additionally, NHalo-4P and NHalo-5P3 recover similar transfer geometries despite NHalo-4P admitting a total maneuver magnitude of $140.2\ m/s$ and NHalo-5P3 requiring a total of $51.6\ m/s$. This difference is likely attributable to NHalo-5P3 possessing a smoother and longer departure arc from the initial orbit, smoother and longer arrival arc onto the target orbit, and alternative maneuver locations. To improve the total maneuver magnitude of NHalo-4P, $w_{Geo} = 0.1$ and $w_{Man} = 0.9$ are instead used to compute a continuous solution from the initial guess. Figure 12 displays the resulting transfer with a total maneuver magnitude of $70.6\ m/s$ and a TOF of 29.2 days. The recovered transfer still resembles the initial guess, demonstrates the ability to effectively prioritize a different balance of objectives in the optimization procedure, and achieves a significant reduction in total maneuver

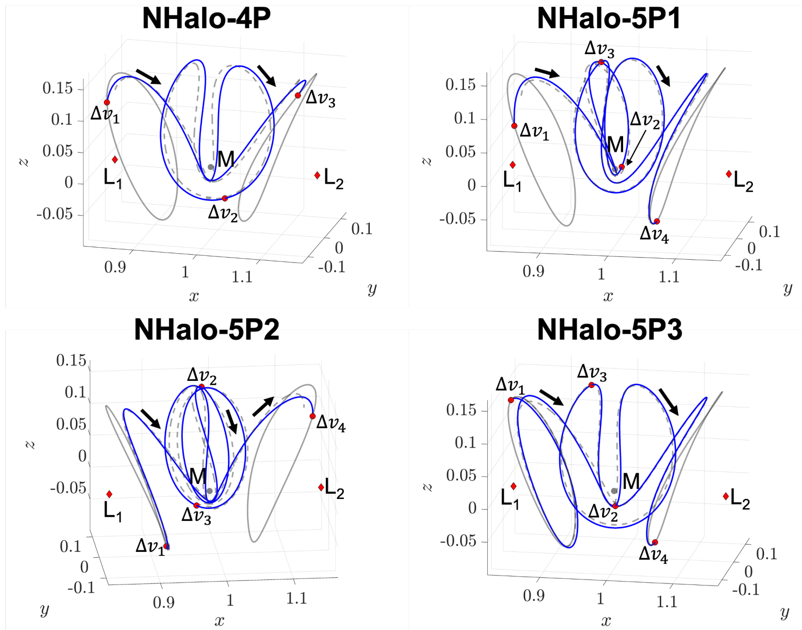

Figure 11. Transfers with distinct geometries between an L_1 and L_2 northern halo orbit in the Earth-Moon CR3BP computed from four- and five-primitive initial guesses.

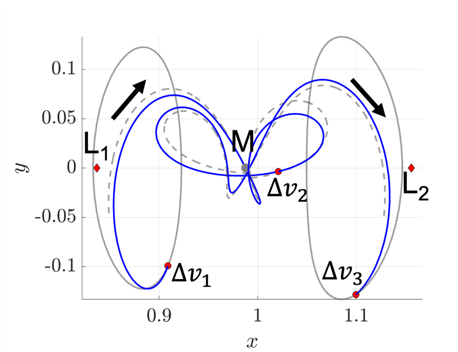

Figure 12. Transfer computed for NHalo-4P using $w_{Geo} = 0.1$ and $w_{Man} = 0.9$ in the optimization procedure.

Table 4. Maneuver magnitudes and time-of-flight (TOF) between the L_1 and L_2 northern halo orbits.

Transfer Name	Δv_1 $[m/s]$	Δv_2 $[m/s]$	Δv_3 $[m/s]$	Δv_4 $[m/s]$	Total Δv $[m/s]$	TOF [days]
NHalo-4P	42.6	44.8	52.8	-	140.2	23.8
NHalo-5P1	55.6	80.7	11.8	9.1	157.2	33.8
NHalo-5P2	14.8	21.6	10.5	54.8	101.7	31.9
NHalo-5P3	19.0	11.1	13.1	8.4	51.6	40.4

magnitude by making large adjustments in the locations of the departure and arrival maneuvers. As a comparison, Haapala recovers a 51.2 day transfer with a similar geometry between two northern halo orbits at similar energy levels, but with a total maneuver magnitude of 11.9 m/s;[31] this difference is due to the use of longer departure and arrival arcs and selection of more efficient maneuver locations. In this paper, impulsive maneuvers are placed between each primitive along the initial guess; however, this comparison motivates our ongoing work to develop improved maneuver placement strategies.

5 CONCLUSION

Motion primitives offer a representation of the fundamental building blocks used to construct more complex motions in a dynamical system. In this paper, a primitive-based initial guess construction framework is presented that enables rapid trajectory design and design space exploration in a multi-body system. First, motion primitives are constructed to summarize periodic orbit families and arcs along stable/unstable manifolds, forming a motion primitive library. Then, a graph is constructed that captures the potential for sequential composability of motion primitives in the library, offering a discrete representation of part of the solution space. The motion primitive graph is constructed in a modular approach and may be tailored based on the level of a priori knowledge possessed by the human designer. Searching this graph produces sequences of motion primitives that support constructing coarse initial guesses for transfers with distinct geometries between an initial and target primitive. These sequences are ranked based on their estimated quality in predicting a nearby transfer. Each distinct sequence supports efficient exploration of the design space to identify transfer solutions with distinct geometries. Next, each primitive sequence is refined to produce an initial guess for a transfer. Direct collocation and multi-objective optimization are then applied to produce continuous maneuver-efficient solutions that geometrically resemble the primitive-based initial guesses. This design procedure is demonstrated by constructing a variety of transfers with distinct geometries in the Earth-Moon CR3BP between an L_1 and L_2 Lyapunov orbit and an L_1 and L_2 northern halo orbit. These examples demonstrate that the motion primitive framework presented in this paper enables rapid initial guess construction for transfers and exploration of the associated design space in a chaotic multi-body gravitational environment.

6 ACKNOWLEDGEMENTS

This work is being completed at the University of Colorado Boulder. It is funded by the NASA Space Technology Research Fellowship from the National Aeronautics and Space Administration. The authors thank Dr. Christopher Spreen and Dr. Robert Pritchett for their support on this work.

REFERENCES

[1] V. Szebehely, *Theory of Orbits: The Restricted Problem of Three Bodies*. London, UK: Academic Press, 1967.

[2] T. R. Smith and N. Bosanac, "Constructing Motion Primitive Sets to Summarize Periodic Orbit Families and Hyperbolic Invariant Manifolds in a Multi-Body System," *Celestial Mechanics and Dynamical Astronomy*, Vol. 134, No. 7, 2022.

[3] T. R. Smith and N. Bosanac, "Using Motion Primitives to Design Libration Point Orbit Transfers in the Earth-Moon System," *AAS/AIAA Astrodynamics Specialist Conference*, Virtual, August 2021.

[4] A. Wolek and C. A. Woolsey, "Model-Based Path Planning," *Sensing and Control for Autonomous Vehicles: Application to Land, Water and Air Vehicles* (T. I. Fossen, K. Y. Pettersen, and H. Nijmeijer, eds.), Vol. 474 of *Lecture Notes in Control and Information Sciences*, pp. 183–206, Springer International Publishing, 2017.

[5] S. M. LaValle, *Planning Algorithms*. Cambridge University Press, 2006.

[6] E. Frazzoli, M. A. Dahleh, and E. Feron, “Maneuver-Based Motion Planning for Nonlinear Systems with Symmetries,” *IEEE Transactions on Robotics*, Vol. 21, No. 6, 2005, pp. 1077–1091.

[7] D. J. Grymin, C. B. Neas, and M. Farhood, “A Hierarchical Approach for Primitive-Based Motion Planning and Control of Autonomous Vehicles,” *Robotics and Autonomous Systems*, Vol. 62, No. 2, 2014, pp. 214–228.

[8] G. A. Tsirogiannis, “A Graph Based Methodology for Mission Design,” *Celestial Mechanics and Dynamical Astronomy*, Vol. 114, 2012, pp. 353–363.

[9] E. Trumbauer and B. Villac, “Heuristic Search-Based Framework for Onboard Trajectory Redesign,” *Journal of Guidance, Control, and Dynamics*, Vol. 37, No. 1, 2014, pp. 164–175.

[10] A. Das-Stuart, K. C. Howell, and D. C. Folta, “Rapid Trajectory Design in Complex Environments Enabled by Reinforcement Learning and Graph Search Strategies,” *Acta Astronautica*, Vol. 171, 2020, pp. 172–195.

[11] N. L. Parrish, “A* Pathfinding Continuous-Thrust Trajectory Optimization,” *AAS 37th Annual Guidance & Control Conference*, Breckenridge, CO, January 2014.

[12] K. L. Bruchko and N. Bosanac, “A Preliminary Exploration of Path Planning for Initial Guess Construction in Multi-Body Systems,” *AAS/AIAA Astrodynamics Specialist Conference*, Virtual, August 2021.

[13] W. S. Koon, M. W. Lo, J. E. Marsden, and S. D. Ross, *Dynamical Systems, The Three-Body Problem, and Space Mission Design*. New York, USA: Springer, 2011.

[14] N. Bosanac, *Leveraging Natural Dynamical Structures to Explore Multi-Body Systems*. PhD dissertation, Purdue University, West Lafayette, IN, 2016.

[15] J. D. Hadjidemetriou, “Resonant Motion in the Restricted Three-Body Problem,” *Celestial Mechanics and Dynamical Astronomy*, Vol. 56, 1993, pp. 201–219.

[16] H. B. Keller, “Numerical Solution of Bifurcation and Nonlinear Eigenvalue Problems,” *Applications of Bifurcation Theory* (P. H. Rabinowitz, ed.), pp. 359–384, New York: Academic Press, 1977.

[17] K. C. Howell, “Three-Dimensional, Periodic, 'Halo' Orbits,” *Celestial Mechanics and Dynamical Astronomy*, Vol. 32, No. 1, 1984, pp. 53–71.

[18] B. A. Conway, *Spacecraft Trajectory Optimization*. New York, USA: Cambridge University Press, 2010.

[19] D. J. Grebow and T. A. Pavlak, “MCOLL: MONTE Collocation Trajectory Design Tool,” *AAS/AIAA Astrodynamics Specialist Conference*, Stevenson, WA, August 2017.

[20] R. E. Pritchett, *Strategies for Low-Thrust Transfer Design based on Direct Collocation Techniques*. PhD dissertation, Purdue University, West Lafayette, IN, 2020.

[21] M. Ozimek, D. J. Grebow, and K. C. Howell, “A Collocation Approach for Computing Solar Sail Lunar Pole-Sitter Orbits,” *The Open Aerospace Engineering Journal*, Vol. 3, 2010, pp. 65–75.

[22] P. Williams, “Hermite-Legendre-Gauss-Lobatto Direct Transcription in Trajectory Optimization,” *Journal of Guidance, Control, and Dynamics*, Vol. 32, No. 4, 2009, pp. 1392–1395.

[23] E. Frazzoli, *Robust Hybrid Control for Autonomous Vehicle Motion Planning*. PhD dissertation, Massachusetts Institute of Technology, Cambridge, MA, 2001.

[24] M. Van der Laan, K. Pollard, and J. Bryan, “A New Partitioning Around Medoids Algorithm,” *Journal of Statistical Computation and Simulation*, Vol. 73, No. 8, 2003, pp. 575–584.

[25] A. A. Paranjape, K. C. Meier, X. Shi, S. J. Chung, and S. Hutchinson, “Motion Primitives and 3D Path Planning for Fast Flight Through a Forest,” *The International Journal of Robotics Research*, Vol. 34, No. 3, 2015, pp. 357–377.

[26] B. Wang, J. Gong, R. Zhang, and H. Chen, “Learning to Segment and Represent Motion Primitives from Driving Data for Motion Planning Applications,” *21st International Conference on Intelligent Transportation Systems*, Maui, HI, November 2018, pp. 1408–1414.

[27] A. Majumdar and R. Tedrake, “Funnel Libraries for Real-Time Robust Feedback Motion Planning,” *The International Journal of Robotics Research*, Vol. 36, No. 8, 2017, pp. 947–982.

[28] J. Han, M. Kamber, and J. Pei, *Data Mining Concepts and Techniques*. Waltham, MA: Morgan Kaufmann Publishers, 3 ed., 2012.

[29] R. M. Holladay and S. S. Srinivasa, “Distance Metrics and Algorithms for Task Space Path Optimization,” *IEEE/RSJ International Conference on Intelligent Robots and Systems*, Daejeon, Korea, October 2016.

[30] A. Wächter and L. T. Biegler, “On the Implementation of an Interior-Point Filter Line-Search Algorithm for Large-Scale Nonlinear Programming,” *Mathematical Programming*, Vol. 106, No. 1, 2006, pp. 25–57.

[31] A. F. Haapala, *Trajectory Design in the Spatial Circular Restricted Three-Body Problem Exploiting Higher-Dimensional Poincaré Maps*. PhD dissertation, Purdue University, West Lafayette, IN, 2014.